Discrete Modeling of Passive Rectifiers in *LCL* Tuned Inductive Power Transfer Receivers

Feiyang J. Lin, *Member, IEEE*, Patrick A. J. Lawton, *Student Member, IEEE*, and Grant A. Covic, *Senior Member, IEEE*

***Abstract*—This article presents a new method of analyzing the performance of the secondary side of an *LCL*-tuned secondary in an inductive power transfer (IPT) system using a passive rectifier. Traditional methods of analyzing such systems simplify the dc load into an equivalent ac load. This approximation skews the phase shifts between the primary and secondary currents and introduces errors in the design stage of the system. The proposed method uses a lookup table (LUT) to characterize the performance of the *LCL*-tuned secondary network. The results are presented and validated at three different power levels (48, 9, and 4 kW). The LUT closely agrees with the measured output powers, phase angles, and coil currents. A sensitivity analysis also shows that it can reduce errors in the simulation by taking practical component variations into account. As such, the proposed LUT characterization method is a valuable tool to quickly determine how an IPT system's design impacts the secondary side's performance in an *LCL*-tuned network with a passive rectifier for IPT systems.**

***Index Terms*—Inductive power transfer (IPT), *LCL* tuning, lookup table (LUT), passive rectifier, phase shift.**

I. Introduction

INDUCTIVE power transfer (IPT) delivers power from a source to a load without a physical connection. IPT is used in various real-world applications, from low-power cell phone charging to high-power applications such as electric vehicle (EV) and airplane charging. It offers several advantages compared to wired charging, such as improved safety and convenience by decoupling the human interaction required to charge a vehicle [1]. It also enables future technologies that will rely on autonomous charging.

A standard IPT system consists of a primary side, which uses an inverter to convert a dc voltage into a high-frequency ac voltage. This voltage is then fed through a resonant tuning network to drive a current in the primary coil that generates a magnetic field. The field couples to a tuned secondary pad in proximity and passes through a secondary rectification stage to produce a dc voltage or current to charge a battery [2].

Manuscript received 8 December 2022; revised 31 January 2023 and 19 March 2023; accepted 28 April 2023. Date of publication 9 May 2023; date of current version 1 September 2023. Recommended for publication by Associate Editor Fei Lu. *(Corresponding author: Feiyang J. Lin.)*

The authors are with the Faculty of Engineering, Department of Electrical, Computer, and Software Engineering, University of Auckland, Auckland 1142, New Zealand (e-mail: jackman.lin@auckland.ac.nz; patrick.lawton@auckland.ac.nz; ga.covic@auckland.ac.nz).

Color versions of one or more figures in this article are available at https://doi.org/10.1109/TPEL.2023.3272645.

Digital Object Identifier 10.1109/TPEL.2023.3272645

EV charging is the primary application of such an IPT system in this article. Here, specific operating conditions are taken from existing standards, such as the SAE J2954 recommendations to ensure backward compatibility [3]. For example, the operating frequency of the system is fixed at 85 kHz. The present standard targets power levels up to 11 kW, so any higher power charging considerations, such as operating voltages and currents, will change for power levels analyzed above this.

A common goal when designing the primary tuning network and inverter is to ensure zero voltage switching (ZVS) operation on the turn-ON edge of the MOSFETs. This switching condition minimized the total energy loss as standard SiC modules have lower turn-OFF loss than turn-ON loss. Reducing this loss is critical to ensuring good system efficiency and to reducing EMI issues due to hard turn-ON.

Common tuning topologies used include the series [4], parallel [5], and the *LCL* network [6], [7]. Here, the *LCL* network includes any partial series compensation, often referred to as *LCC* compensation in the existing literature [8]. The most common system topologies are the series-series (SS) [9], [10], the *LCL*-parallel (*LCL*-P) [11], and the *LCL–LCL* systems [8], [12], given that these present a current source to the battery load.

SS systems are often used in low-power applications due to their simplicity. However, they have challenges in higher-power applications as the load and resonant currents must be equal, so switching harmonics are not as easily suppressed. For a given dc bus voltage (V_{bus}), the inverter current grows higher as power demands increase, which leads to more expensive switches.

Industrial systems generally prefer *LCL* topologies on the primary side because the inverter inductor decouples the load current from the resonant current and acts as a band-pass filter to the switching harmonics [13]. This topology reduces the cost of the switches and allows the primary current to be kept constant regardless of load. However, it comes at the cost of needing an additional inductor, leading to higher costs and weight. This article focuses on the *LCL–LCL* system as it aims to push the power output to 50 kW.

Characterizing the performance of primary inverters becomes challenging as the loading conditions change with power and misalignment, more so if the secondary side uses a passive rectifier. The typical approach in most designs is to assume that the secondary rectifier does not go into discontinuous conduction mode (DCM). This allows the designer to simplify any battery load into an equivalent ac load resistor and allows the IPT system to be analyzed using first harmonic analysis (FHA).

As such, certain assumptions on scalability are made under particular operating conditions. The theory is validated by running a detailed simulation model using either LTSpice or PLECs once rough values are achieved. However, this means that to characterize an inverter throughout its entire operational range based on aligned and misaligned magnetics and over various power output requirements requires hundreds of thousands of simulations, each specific to the use case. Existing research papers such as [14], [15], [16], [17], and [18] either use FHA with fully conducting rectifiers, or investigate only series-series systems.

In [19], FHA is used to analyze the IPT system. The result of the FHA analysis is then used to approximate the load and the impact of DCM of the passive rectifier on the output power.

In [20], the impact that a combination of tuning topologies has on the primary and secondary sides with regard to the stability of the IPT system is studied. This article also uses FHA to determine the reflected impedance but does not analyze the *LCL–LCL* system.

Analytical methods have been proposed to analyze the secondary passive rectifier. In [21], a series-series compensated system is modeled in the time domain. This work shows that it is possible to model the passive rectifier through an iterative mathematical process. However, it does not consider more complex tuning topologies such as the parallel or *LCL*-tuned systems.

A method to control the conduction state of the rectifier is to use an active rectifier. Here, diodes on the secondary side are replaced with actively switching MOSFETs [22], [23], [24]. Active rectifiers allow the secondary inverter voltage to be controlled at a defined phase with respect to the primary inverter voltage. This method eliminates DCM as the diodes are forced to conduct, but at an additional cost compared to passive systems. Wirelessly synchronizing the primary and secondary converters is also challenging.

The real power transfer in an IPT system is defined by the volt-amps in the primary and secondary pads, as well as the phase shift between the currents in the coils (θ_{12}). It is challenging to predict how a passive rectifier impacts θ_{12} in an *LCL*-tuned secondary as it can go into DCM under certain loading conditions. This introduces additional harmonics into the system, which need to be accounted for.

The primary goal of this article is to simplify the design process by investigating the use of a lookup table (LUT) to characterize the secondary side of the system for the *LCL–LCL* tuned topology. This article does not derive a mathematical model for the passive *LCL* rectifier due to its complexity. This method predicts the phase shift between the primary and secondary currents (θ_{12}). The LUT reduces the number and complexity of simulations needed to analyze the performance of the secondary side and allows engineers to converge to a desired solution much faster than is currently possible. Any such table will only need to be generated once and is generally agnostic to changes in magnetic parameters. The initial LUT is designed using ideal parameters as it is challenging to predict component variations in the design stage of an IPT system. An additional analysis is included to show the impact of parameter drift.

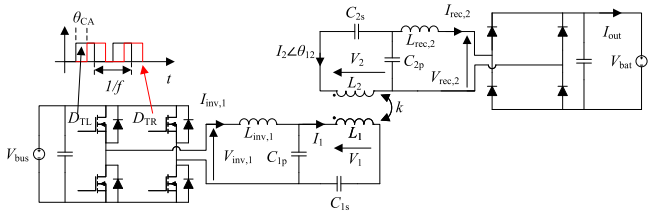

Fig. 1. Full *LCL-LCL* tuned IPT system with passive rectifier output into a battery. Parasitic elements such as lead inductances (L_{lead}) and ESRs not shown.

This article first presents the fundamental design methodologies for IPT systems. It then justifies and details the approach required to model the secondary passive rectifier. Practical measurements show that the methodology can predict operation to within 5% accuracy when comparing a practical system to an ideally tuned system. A sensitivity analysis is also given, which investigates how mistuning impacts the desired characteristics of the practical system. Finally, conclusions are given.

II. Standard IPT System Design

A standard IPT system without any parasitic elements included is shown in Fig. 1. This work uses an *LCL–LCL* network, driven by an H-bridge on the primary side and is passively rectified on the secondary side into a battery with a range of voltages (V_{bat}) depending on its state of charge (SOC). Practical secondary sides often require a form of regulation in order to control I_{out}. Such regulation techniques include buck, boost, buck–boost, or synchronous converters. All such converter types transform the impedance presented by the battery. This work does not focus on the regulatory aspects of the system.

This section covers each component and explains how it is chosen or derived. The most common inverter topology is an H-bridge, which allows full phase and duty cycle control with the fewest MOSFETs. As noted earlier, the *LCL* tuning topology is preferred due to its ability to generate a constant current source in the primary coil.

The primary side consists of an inverter inductor ($L_{\text{inv},1}$), a primary parallel capacitor ($C_{1\text{p}}$), and the primary coil itself L_1. A partial series capacitor $C_{1\,\text{s}}$ is also often used to help achieve the desired primary current. The components are nominally chosen for an unloaded system according to the following:

$$\omega L_{\text{inv},1} = \frac{1}{\omega C_{1\text{p}}} = \omega L_1 - \frac{1}{\omega C_{1\,\text{s}}}. \tag{1}$$

The values of the primary passive elements are set by the dc input bus voltage (V_{bus}) and a conduction angle (θ_{CA}) in radians between the two half-bridges. The fundamental of this stepped waveform combined with the tuned *LCL* network sets the unloaded primary current (I_1) as described in the following:

$$I_1 = \frac{V_{\text{bus}} 2\sqrt{2}}{\pi \omega L_{\text{inv},1}} \sin\left(\frac{\theta_{\text{CA}}}{2}\right) \tag{2}$$

The secondary side also needs compensation, and available options include series, parallel, or *LCL* networks. The *LCL* network is preferred for higher power levels. The challenge

in modeling the secondary side is to consider the impact of a passive rectifier on the loading condition as it introduces higher order voltages and current harmonics, which introduce additional VARs into the system that is difficult to quantify analytically.

The chosen *LCL*-tuned secondary side consists of a rectifier inductor ($L_{rec,2}$), a secondary parallel capacitor (C_{2p}), and the secondary coil L_2. A partial series capacitor $C_{2\,s}$ is also used to achieve the desired output characteristics required to charge a battery at any given voltage. These components are usually chosen according to a similar method as the primary side, as shown in the following:

$$\omega L_{\mathrm{rec},2} = \frac{1}{\omega C_{2\mathrm{p}}} = \omega L_2 - \frac{1}{\omega C_{2\,\mathrm{s}}}. \tag{3}$$

A. Key IPT Equations

Key design parameters for the magnetic system include the inductances of the two coils and various coupling factors (k) between them based on the secondary position. Factors that govern the amount of power transfer includes the current in the primary and secondary coils and the loading condition of the secondary side.

When the primary coil is energized with some current set by V_{bus} and θ_{CA}, it will have a volt-amp product equal to VA_1 as defined as follows:

$$VA_1 = |V_1 I_1|. \tag{4}$$

This VA_1 can be used to calculate the uncompensated volt-amps of the secondary pad (S_{U}). Here, S_{U} is proportional to the coupling factor (k) between the two coils in a standard IPT system as shown in the following. It is also equal to the product of the induced open circuit voltage (V_{oc}) and the short circuit current (I_{sc}) in the secondary coil

$$S_{\mathrm{U}} = k^2 VA_1 = |V_{\mathrm{oc}} I_{\mathrm{sc}}|. \tag{5}$$

The rms value of V_{oc} is defined in (6), while I_{sc} is proportional to both V_{oc} and the impedance of the secondary coil in (7)

$$V_{\mathrm{oc}} = j\omega k\sqrt{L_1 L_2} I_1 \tag{6}$$

$$I_{\mathrm{sc}} = \frac{V_{\mathrm{oc}}}{\omega L_2}. \tag{7}$$

If a partial series compensation network is used to boost the short circuit current, then the power analysis should use a boosted short circuit current I'_{sc}. This parameter is defined as follows and is related to the series compensated impedance (X'_2):

$$I'_{\mathrm{sc}} = \frac{V_{\mathrm{oc}}}{\omega L_2 - 1/j\omega C_{2\,\mathrm{s}}} = \frac{V_{\mathrm{oc}}}{X'_2}. \tag{8}$$

The magnetic parameters of an IPT system are generally quantified early in the simulation stage. L_1 and L_2 are given a nominal value, and k has a range defined by the allowable pad misalignment. Equation (2) and the *LCL* tuning topology also nominally hold the I_1 constant. This means that V_{oc} has a certain defined range.

The secondary coil also has a current (I_2) in it with some phase with respect to the primary current ($\angle\theta_{12}$). The secondary coil volt-amp product (VA_2) is defined by the following:

$$VA_2 = |V_2 I_2|. \tag{9}$$

Finally, the ac output power supplied by the secondary coil $P_{\mathrm{o,ac}}$ is defined in the following:

$$P_{\mathrm{o,ac}} = k\sqrt{VA_1 VA_2}\sin(\theta_{12}). \tag{10}$$

A higher $P_{\mathrm{o,ac}}$ correlates to a higher P_{out} if the efficiency can be assumed to be relatively consistent. In the initial stages of this work, the only losses considered are in the parasitic elements. At the same time, the diodes used in the secondary rectifier are modeled as lossless elements for simplicity.

Not included in Fig. 1 are the equivalent series resistances (R_{esr}) of each of the passive components in the system. Low ESRs are critical to ensure high unloaded quality factors (Q), which are desired to minimize the copper and core losses in the inductors and the resistive losses in the capacitors. These resistances depend on the types and the quality of the construction of each component in the network. As an example, ceramic capacitors used in the tuning network tend to have very low R_{esr}. These components have high unloaded quality factors, $Q_{\mathrm{C,UL}}$ (11), typically in the 2000 s. However, inductors will have unloaded quality factors ($Q_{\mathrm{L,UL}}$) of approximately 400 due to the natural constraints of winding a coil with fixed conductivity (12), and additional losses introduced by ferrite and aluminum, which also cause the ESRs to rise

$$Q_{\mathrm{C,UL}} = \frac{1}{\omega C R_{\mathrm{esr}}} \tag{11}$$

$$Q_{\mathrm{L,UL}} = \frac{\omega L}{R_{\mathrm{esr}}}. \tag{12}$$

III. Passive Secondary Rectifiers in IPT Systems

The challenge in the design of IPT systems with passive rectifiers is to reliably predict θ_{12} as both k and V_{bat} vary. As discussed, θ_{12} determines the input power, so the real power output can be predicted accurately for any given volt-amp effort.

If θ_{12} is known, then the reflected impedance (X_{ref}) and load (R_{ref}) that the secondary pad presents to the primary can be characterized by (13) and (14). Here, X_{ref} is inductive when θ_{12} is less than $\frac{\pi}{2}$, and capacitive otherwise

$$X_{\mathrm{ref}} = j\omega k\sqrt{L_1 L_2}\left|\frac{I_2}{I_1}\right|\cos(\theta_{12}) \tag{13}$$

$$R_{\mathrm{ref}} = \omega k\sqrt{L_1 L_2}\left|\frac{I_2}{I_1}\right|\sin(\theta_{12}). \tag{14}$$

The impact of parameters such as θ_{12} and reflected voltages changes the reflected load on the primary converter. This article does not investigate how this causes the primary converter switching characteristics to change. The focus of this article is to simplify the secondary side's modeling and prove that the proposed method provides good accuracy for passively rectified *LCL* secondaries. As such, the primary side can be assumed to consist of an *LCL*-tuned network which provides a controlled constant current source into the primary coil.

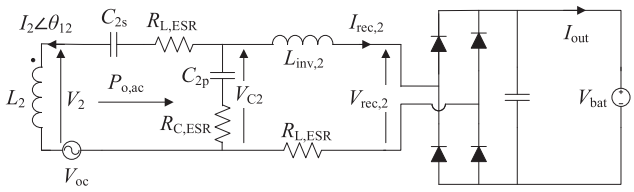

Fig. 2. Decoupled secondary side used to generate the lookup table for the passive secondary rectifier.

Here, as in many practical systems, L_1 and L_2 are assumed to be set by the designer. I_1 can be designed by a combination of components as discussed in (1) and (2). k has a range of values set by the magnetic design. The two variables that need to be determined precisely are $|I_2|$ and θ_{12} to solve (10) and better understand the power throughput of the IPT system.

The primary and secondary sides can be split into two distinct systems, which can be solved separately. Equation (6) shows that V_{oc} always leads I_1 by $\pi/2$ radians. This allows the secondary side to be modeled using a voltage source as shown in Fig. 2, and θ_{12} is defined as 90° less than the phase shift between V_{oc} and I_2.

Various assumptions, such as a secondary rectifier that is always conducting and low harmonic content in the primary and secondary currents allow designers to perform a first harmonic analysis of the system and derive approximate power and loss analysis of systems. Under this assumption, $V_{rec,2}$ is a square wave with an rms value that is $\pi/(2\sqrt{2})$ times higher than V_{bat}. Here, the diodes are assumed to have a much lower forward voltage drop compared to the battery voltage. Considering the power balance on either side of the rectifiers, the output current (I_{out}) is $2\sqrt{2}/\pi$ times lower than the rms of the secondary rectifier current ($I_{rec,2}$). For a perfectly tuned system, the rms value of $I_{rec,2}$ is equal to the rms value of I'_{sc} (8).

The assumption of a fully conducting rectifier and a first harmonic analysis allows designers to scale their designs from expected values. For example, suppose V_{bat} is the only parameter that is varied and is decreased from 800 to 600 V. In that case, this approach allows designers to calculate a power drop from full power at 800 V to 3/4 of full power at 600 V. Likewise, if V_{oc} is doubled (because k or I_1 doubles), then the output power is expected to also double. This article shows that these relationships do not hold for all cases because the secondary rectifier does not remain in continuous conduction for all practical values of k, which vary as the IPT system becomes misaligned. The V_{bat} will also have a range of voltages based on its SOC, and therefore an increase in the battery voltage can also cause the rectifier to go into discontinuous mode.

The required parameters for the LUT are the gains between V_{bat} and V_{oc} (G_V), and the gain between the partially tuned impedance X'_2 and V_{oc}, as defined in (8) (Y). These are defined in the following as:

$$G_V = \frac{V_{bat}}{V_{oc}} \tag{15}$$

$$Y = \frac{X'_2}{V_{oc}}. \tag{16}$$

In the initial study, the system is assumed to be ideally tuned according to (3). In this article, the design space is for a 50 kW system. However, the LUT can be used for any power design and does not need to be repopulated.

A. Lookup Table

An ideally tuned system shown in Fig. 2 was simulated using PLECs over the search space of interest and the results are plotted in Fig. 3. A normalized simulation set was performed with $V_{oc} = 1$ V. G_V was analyzed in a range between 0.2 and 4, and Y was analyzed in a range between 0.004 and 0.05. The dataset range presented in this article is chosen as it is relevant to the power levels in a system that ranges between 4 and 50 kW. The system is also applicable for lower power levels, but typically inverters are operated from 10% to 100% for efficiency reasons. As such, results are kept nominally within this range for clarity of the article.

Here, the unloaded Q factors of the secondary side components are kept constant as the pad impedances and tuning values vary, which is generally expected with good designs. This ensures that the ESRs of the pads do not interfere with the power transfer of the system and a system with abnormal losses is not investigated. Thus, $R_{L,ESR}$ and $R_{C,ESR}$ are changed throughout the search space. $Q_{C,UL}$ is initially assumed to be 2000, and $Q_{L,UL}$ is assumed to be 400. A sensitivity analysis will be presented in Section V to investigate how variations in component values and parasitic elements impact the modeling of the system.

Fig. 3(a)–(c) show how certain critical operating parameters vary as Y and G_V change. Fig. 3(a) shows the normalized output power (P_{out}) per volt of V_{oc} (W/V), where $P_{out} = V_{bat}I_{out}$. Here, P_{out} increases as Y becomes smaller, or as G_V becomes larger. This is expected because a lower Y value directly means that X'_2 is smaller or V_{oc} is increasing, resulting in a larger I'_{sc}. As I_{out} is related to I'_{sc}, a lower Y logically results in a higher output power. Similarly, as G_V increases, the output voltage also grows larger. Thus for any system where all of the other factors are fixed, P_{out} should logically grow larger as V_{bat} increases.

Fig. 3(b) shows that θ_{12} does not vary as Y varies. Instead, θ_{12} only depends on G_V. As G_V increases, θ_{12} decreases. For the *LCL*-tuned network θ_{12} approaches 90° as G_V approaches 0. This makes sense as P_{out} approaches 0 in this case, and only the resonant currents exist on the secondary side. It also shows that the *LCL*-tuned secondary network always reflects an inductive load on the primary side.

For a constant V_{oc}, Fig. 3(c) shows how the secondary resonant current varies with changes in Y and G_V. Here, I_2 does not need to be denormalized, so the current can be read directly off the graph for any given power level.

As shown in (10), the input power (and therefore P_{out}) increases as θ_{12} approaches $\pi/2$. This happens as G_V becomes smaller, as shown in Fig. 3(b). However, this also means that the P_{out} per V_{oc} and I_2 shown in Fig. 3(a) and (c) decreases as θ_{12} increases. A careful balance of the magnetic system at the design stage is necessary since G_V varies with V_{oc}, which is related to k and I_1. Balance can be achieved by carefully considering the

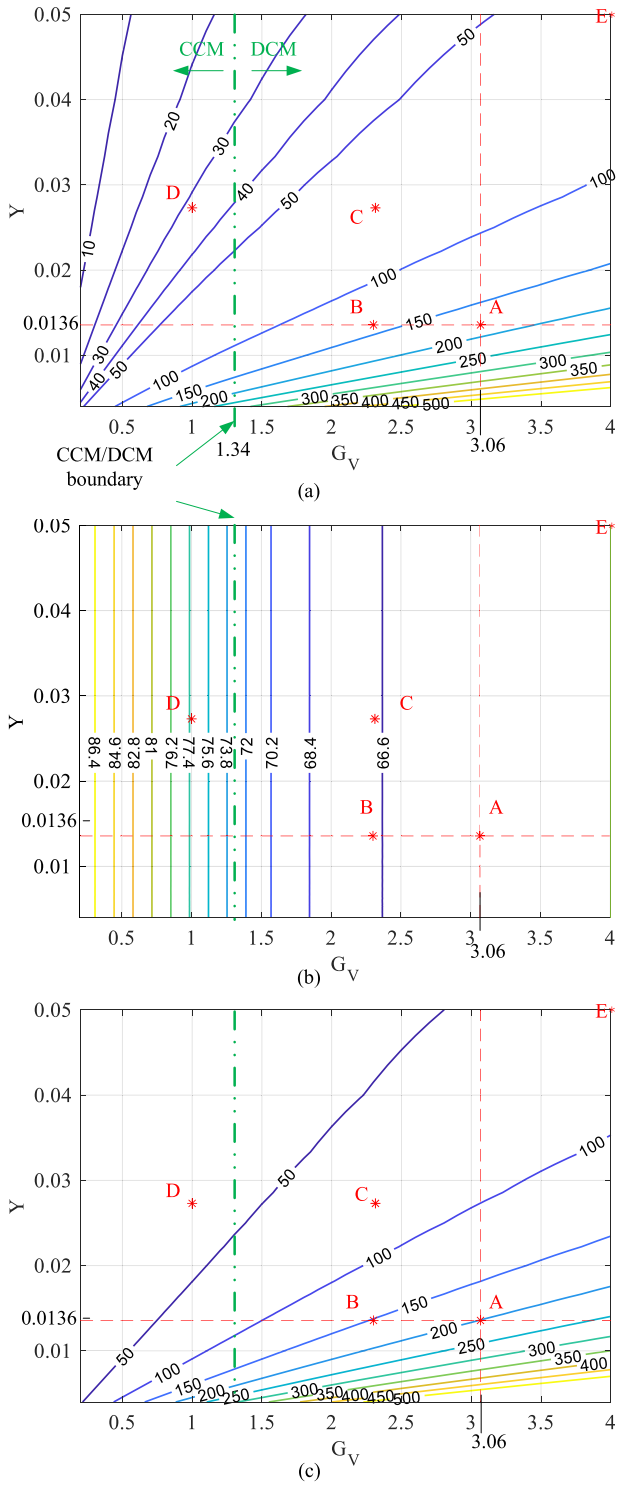

Fig. 3. LUT for the ideally tuned *LCL* passive secondary rectifier showing the (a) P_{out} per V_{oc} (W/V) (b) θ_{12} (rad), and (c) I_2 (A) as both Y and G_{V} are varied.

volt-amp requirements in both the primary and secondary sides, which are influenced by various design choices such as tuning values, input bus voltages, conduction angles, etc. Since this article focuses on an LUT analysis of the secondary side only, the magnetic design of the IPT system is not covered in detail.

TABLE I
IDEAL AND PRACTICAL MAGNETIC PARAMETERS

Measured magnetic parameters			
L_1	18.2 μH $\pm$ 0.32%	L_2	17.3 μH $\pm$ 0.43%
$L_{1,\text{lead}}$	1.8 μH	$L_{2,\text{lead}}$	1.04 μH
k_{12}	0.133		
I_1	207 A	I_2	204 A
Ideal tuning values			
$L_{\text{inv},1}$	6.684 μH	$L_{\text{rec},2}$	6.629 μH
$C_{1\text{p}}$	524.5 nF	$C_{2\text{p}}$	528.9 nF
$C_{1\text{s}}$	262.8 nF	$C_{2\text{s}}$	302.1 nF
Practical tuning values			
Parameter	Value	Parameter	Value
$L_{\text{inv},1}$	7.5 μH	$L_{\text{rec},2}$	7.4 μH
$C_{1\text{p}}$	536 nF	$C_{2\text{p}}$	533 nF
$C_{1\text{s}}$	263 nF	$C_{2\text{s}}$	304 nF

Instead, any changes in k or I_1 are abstracted into the expected variations in V_{oc}.

B. Interpreting the LUT

This section gives an example of how to use the proposed LUT to aid in designing an *LCL–LCL* tuned IPT system.

Instead of analyzing the system at any particular k or I_1, the points of interest will be analyzed at various V_{oc}'s, and G_{V} is determined by the ratio shown in (15).

For the initial study, an existing 50 kW pad designed in [12] is used to test the model's validity. The IPT system described in this article consists of a circular primary pad and a circular receiver pad, both *LCL*-tuned. In the 50 kW evaluation presented, the input and output are connected so that the dc power supply only supplies the losses during a 50 kW power transfer test. Thus, there is a limitation on the existing test system where $V_{\text{bat}} = V_{\text{bus}}$. For lower power tests ($\leq$ 10 kW), decoupling these two voltages is possible as the appropriate power supplies and loads become available. Practical validations will be presented in Section IV.

The magnetic parameters of the 50 kW system are given in Table I. Note that practical tuning values deviate slightly from ideal tuning values. In this section, a set of ideal tuning values will be calculated for the initial analysis. Furthermore, additional parasitic inductances are introduced by the leads (L_{lead}) that are physically required to connect the pads to the tuning topology. These were measured to be approximately 1.8 μH for the primary side and 1.04 μH for the secondary side. This means that the compensation network needs to be designed for a total inductance of $L_{1\text{or}2} + L_{\text{lead}}$. However, the actual volt-amp generation is defined by only L_1 or L_2 for the primary and secondary sides, respectively.

Point A in Fig. 3(a)–(c) shows the operating condition as indicated using the magnetic parameters given in Table I. This point represents the nominal operating condition of the secondary rectifier in the k_{12} position. The ideal system shown in [12] is placed at k_{12} so $|V_{\text{oc}}| = 260.90\ \text{V}_{\text{RMS}}$, $V_{\text{bus}} = V_{\text{bat}} = 800$ V, giving a $G_{\text{V}} = 3.066$. Furthermore, due to the partial series tuning and the induced V_{oc}, $Y = 0.0136$. The normalized LUT in

TABLE II
COMPARISON OF THE IDEAL NORMALIZED MODEL TO A DENORMALIZED AND A FULL SYSTEM MODEL AT POINT A IN FIG. 3

	Normalized	Denormalized	Full model
V_{oc}	1	260.9	261.57
G_V	3.066	3.066	3.058
Y	0.0136	0.0136	0.0136
V_{bat}	3.066	800	800
X_2'	0.0136	3.5401	3.5401
I_2 (A)	200.9	200.9	200.586
θ_{12} (°)	65.67	65.60	69.97
P_{out} (kW)	0.179	46.70	46.23
$P_{o,ac}$ (kW)	N/A	N/A	48.208

Point A in this Fig. 3(a)–(c) shows a power gain of 170.20 W/V, $\theta_{12} = 65.66°$, and $I_2 = 209$ A.

Fig. 3 also shows the boundary between CCM and DCM, which occurs at approximately $G_V = 1.34$. Fig. 3(b) shows that the DCM boundary occurs when $\theta_{12} = 73°$. According to (10), this corresponds to a 4.4% power drop, despite remaining in CCM. The output power per volt increases if G_V increases further, but this comes at the cost of operating at a lower θ_{12}, causing the efficiency of the system to drop. For example, if the system operates at $G_V = 3$, then $\theta_{12} = 66.4°$, so for a fixed coupling and pad VAs, the output power will drop by 14% compared to the ideal scenario of $\theta_{12} = 90°$.

Table II shows a comparison of the proposed normalized LUT, the denormalized result using the predicted $V_{oc} = 260.90$ V (both simulated using the secondary only model shown in Fig. 2), and the values provided by a final simulation using the whole IPT system as in Fig. 1. This table shows that the P_{out} of a system with practical values can be predicted by multiplying the normalized model value by the expected V_{oc}. The predicted value also has a close agreement with the full model. The phase shift between the primary and secondary currents has a very small variation between all three modeling methods of approximately 0.3°, which is practically insignificant.

Since the normalized and denormalized analysis only use a voltage source to model V_{oc}, there is no primary source to supply $P_{o,ac}$. However, the full model (see Fig. 1) has an *LCL*-tuned primary network, so there is a defined I_1 and k. As such, a theoretical $P_{o,ac}$ can be calculated using (10)

This shows the ideal model for a rectifier using an LUT is accurate and can be used to predict various operational parameters on the secondary side without needing to perform the full simulation at each position of interest.

C. Application of the LUT

The above work presented in this article shows that the proposed LUT method of analyzing a passive full bridge rectifier in an *LCL–LCL* IPT system is accurate and can be used to predict P_{out}, θ_{12}, and I_2. This section describes how this information can be used to quantify the performance of the secondary side as the input or output parameters are changed.

V_{bat} will realistically have a voltage swing over a nominal range for any battery charging application. For this article, this is assumed to be between 600 and 800 V. The change in battery voltage can be visualized along points A to B in Fig. 3 for a constant k. As discussed earlier, the typical assumption made in the design of IPT systems is that $I_{out} = (2\sqrt{2}/\pi)I_{sc}$ for a perfectly tuned *LCL* system where the passive rectifier is always operating under continuous conduction. In this case, if V_{bat} drops from 800 to 600 V, then the P_{out} should scale down to 35.02 kW. However, using the LUT shows that the $P_{out} = 35.85$ kW when the V_{bat} is decreased to 600 V, which is 830 W higher than the standard simplified extrapolation.

The LUT method can accurately predict the output power when operating conditions are changed faster and provides more accurate information than conventional methods, such as running various simulations or scaling based on assumed parameters. This method can also provide designers with accurate knowledge of θ_{12}, which is a critical design parameter for further work involving primary side design.

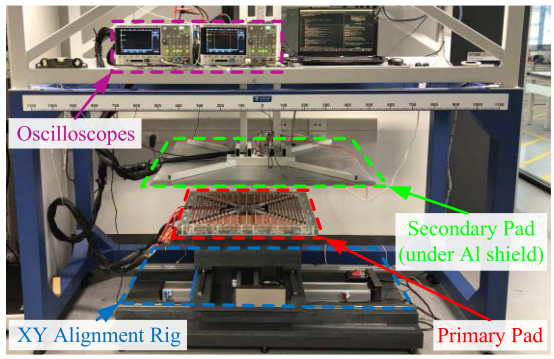

(a)

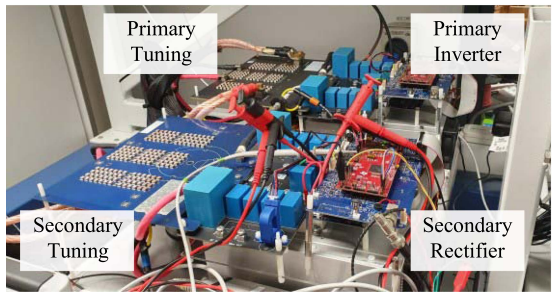

(b)

Fig. 4. Photographs of the experimental set up including the (a) magnetic couplers used and the alignment system, and (b) the inverter and rectifier used in the set up [located behind the oscilloscopes shown in (a)].

IV. PRACTICAL VALIDATIONS

The system was validated using the existing pads on the alignment rig as shown in [12] and is shown in Fig. 4. Here, the nominal target P_{out} at point A in Fig. 3 is 50 kW. In [12], no more than 45.9 kW was achieved as the initial design procedure did not account for the impact of θ_{12}. The theoretical analysis in this article has proven that θ_{12} should be approximately 65.66°. The system parameters are presented in Table I. As noted earlier, V_{bus} and V_{bat} are linked. The dc supply (Keysight N8957 A) only provides the losses in the system. The waveforms of interest are I_1, I_2, V_{bat} (shown on the oscilloscope as V_{out}), and I_{out}. Here, I_1 is used as a reference current to get a measurement for θ_{12}.

TABLE III
DIFFERENT APPLICATIONS OF THE LUT FOR POSITIONS A, B, C, AND D SHOWN IN FIG. 3, USING DENORMALIZED VALUES

Simulated denormalized values					
	A	B	C	D	E
X_2'	3.54	3.54	3.54	3.54	3.54
V_{oc}	260.9	260.9	129.7	129.7	68.5
V_{bat}	800	600	300	129.670	274
Y	0.0136	0.0136	0.0273	0.0273	0.05
G_V	3.066	2.300	2.314	1	4
I_2 (A)	200.59	152.21	76.38	33.31	70.14
P_{out} (kW)	46.70	35.84	8.93	4.16	4.26
θ_{12} (°)	65.67	66.74	66.69	78.74	65.38
Practically measured values*					
I_1 (A)	205.99	N/A	102.84	101.93	55.13
I_2 (A)	203.15	N/A	76.77	33.93	67.96
V_{oc}	258.09	N/A	128.85	127.71	69.07
P_{out} (kW)	48.00	N/A	9.33	4.16	4.24
θ_{12} (°)	66.92	N/A	69.90	77.46	66.61

*practical values measured at $M = k\sqrt{L_1 L_2} = 2.346\ \mu$H

These are plotted in Fig. 5(a)(i). The rms values of I_1 and I_2 are given and show good agreement with the theoretical values in Table III.

There are a few errors caused by the resolution of either the probes or the oscilloscopes based on the chosen measurement scales, as well as practical differences between the ideal and constructed tuning components. This section will compare the accuracy of the measured values against the ideal LUT as presented in Fig. 5. Section V will investigate how mistuning impacts the performance of the system.

One such example is shown in Fig. 5(a)(i), where the oscilloscope shows V_{bus} and V_{bat} at 780 V instead of the set 800 V. These sorts of measurement errors are accounted for by verifying other parameters, such as the track and inverter currents. These measurements align closely with simulated values so small errors in measurement are easily accounted for.

Similarly, there are phase measurement errors as current probes (Ragowski probes) have difficulty measuring phase to a precise value. DC current clamps also inherently have measurement errors, and the results presented are given after careful calibration. The dc output current is measured using a Hioki 3274 clamp probe.

The measured $P_{out} = 48$ kW and is higher than the predicted 46.7 kW from the denormalized model presented in Table II. This is due to the imperfect tuning values in the practical system, as shown in Table I. The measured value is only 2.8% higher and is well within any margin of error. Furthermore, the measured θ_{12} also closely agrees with the simulated values, deviating by only 1.15°.

Point B could not be validated as the equipment to deliver 36 kW with different V_{bat} and V_{bus} voltages was unavailable. Instead, Point C was chosen as another point to be validated. This point was chosen as G_V is almost the same as point B. Therefore, θ_{12} should be very similar in both cases, despite much lower power transfer. Since V_{oc} is halved, Y will double for the same tuning topology on the secondary side. The power delivery available is now dictated by the dc power supply (Keysight N8957 A), which can supply up to 15 kW to the bidirectional power supply acting as a load (Regatron G5.RSS). Here, V_{bat} is chosen to be 300 V, V_{bus} is set at 400 V, and $V_{oc} = 128.85$ V.

Fig. 5(b)(i) and Table III show that the I_2s agree closely with simulations. Here, there is once again a higher power transfer in measurement compared to simulation by approximately 4.3%, which is within the acceptable margin of error.

The phase error is small, just 3° (69.94° versus the simulated 66.69°). The measurement and simulated value error is +4.8% and is within the acceptable tolerance.

Point D [shown in Fig. 5(c)(i)] was chosen as a third validation point to show that a low G_V, with no other changes in the system compared to point C will cause θ_{12} to increase. G_V is intentionally set at approximately 1. As expected, the output power drops, but the LUT and measured results are in close agreement. There is also a minimal error in the predicted and measured power values since mistuning has a smaller absolute impact on the errors.

Fig. 5(d)(i) shows an extreme operating point where $G_V = 4$ and $Y = 0.05$. The measured P_{out}, θ_{12}, and I_2 all agree closely with the ideally simulated values. Furthermore, Fig. 5(d)(ii) shows the primary and secondary bridge voltages and currents. Here, $V_{rec,2}$ (shown in blue), is in DCM. However, the practical nature of the body diodes in the switches causes some reverse recovery which forces the voltages at the switching edges to commutate. This phenomenon also exists in previous work [19]. Combined with the results Fig. 5(a)(ii), this proves that the proposed method is accurate even in DCM. Fig. 5(b)–(c)(ii) prove that the method is also valid for CCM operating conditions.

The four experimental points also show the validity of the DCM boundary presented in Fig. 3. Here, only point D [see Fig. 5(c)] is expected to operate under CCM, and the rest of the operating conditions are in DCM. The experimental validations shows this is true, and that as G_V grows from point C to A to E [see Fig. 5(b) to (a) to (d)], the discontinuity becomes increasingly pronounced.

Finally, Fig. 5(a)–(d)(ii) show that the system operates under ZVS turn-ON conditions under these various operating conditions.

A. Practical Applications

All of the results shown prove that the measurements and the simulations have an acceptable agreement. The LUT method can give an idea of what to expect from the secondary side as the operating conditions vary within 5% accuracy. The advantage of this method is the ability to quickly determine the expected output power and θ_{12} without additional time-consuming simulations.

The results presented here can be used to predict the θ_{12} between the primary and secondary coil currents. This is powerful as it simplifies the operation of the complex secondary network into an $I_2 \angle \theta_{12}$ factor, allowing designers to predict a range of reflected impedances and resistances to design primary inverters more quickly. As this is beyond the scope of this work, it is not discussed in further detail.

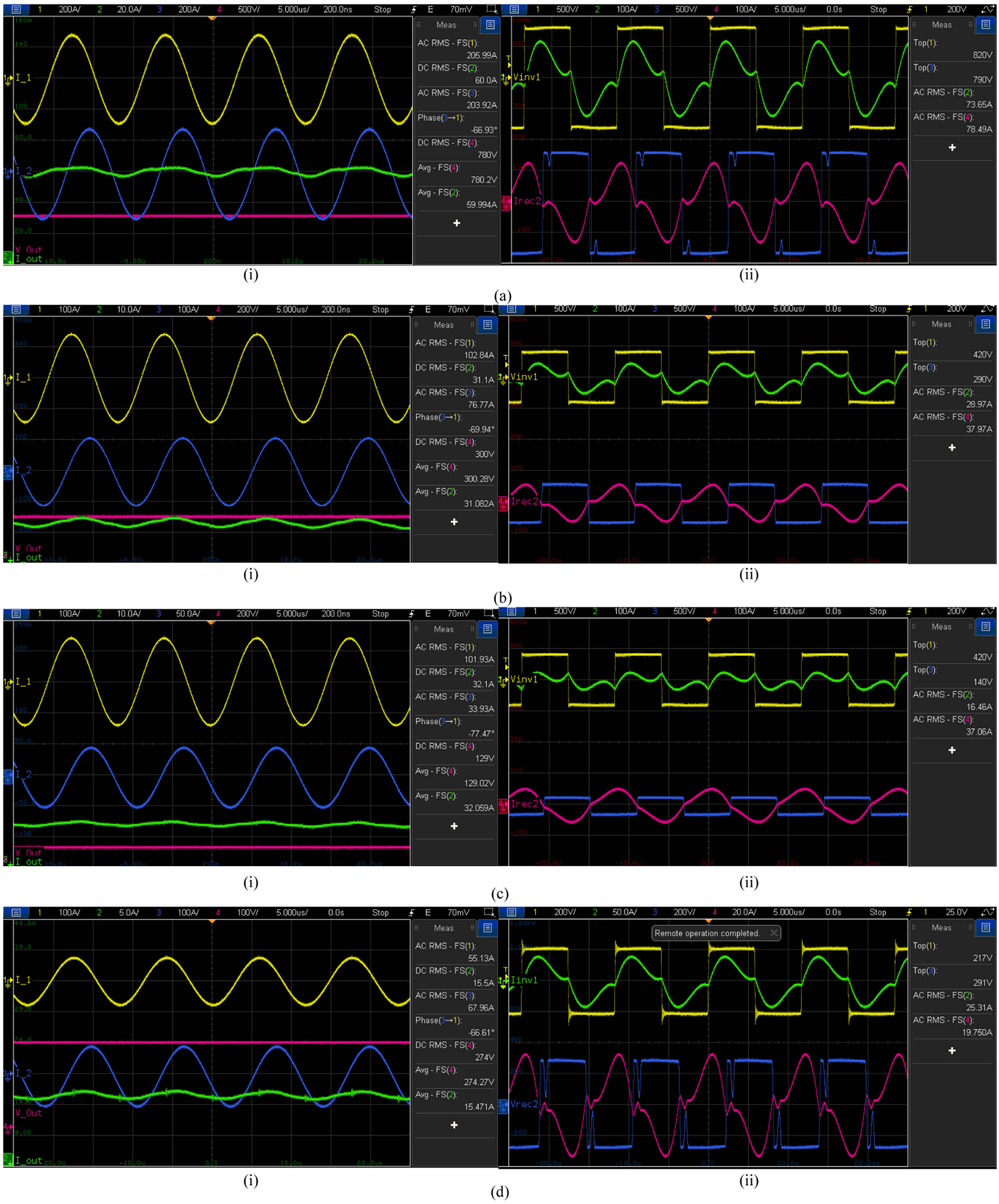

Fig. 5. Practical validation of the system at (a) point A, (b) point C, (c) point D, and (d) point E as shown in Fig. 3 and Table III. (i) shows the the track currents I_1, I_2, and the output voltages and currents V_{bat} and I_{out}. (ii) shows the inverter and rectifier voltages and currents $V_{\text{inv},1}$, $I_{\text{inv},1}$, $V_{\text{rec},1}$, $I_{\text{rec},1}$.

The next section discusses how the secondary tuning network's mistuning impacts the measurements' accuracy.

V. Model Sensitivity to Mistuning

The previous section discussed the accuracy of ideally tuned systems using the proposed LUT method. Such assumptions are difficult to achieve due to component tolerances and variations in parasitic parameters as operating conditions change. It is unlikely that mass-produced systems are perfectly tuned when assembled and are also likely to drift over time, despite good quality control.

In this work, the only parameters where sensitivity needs to be analyzed are the passive components on the secondary side. This section uses PLECs to simulate the proposed system at Points A, C, and D measured in Table II. Shifts in P_{out} and θ_{12} with variations in either unloaded Q or the component values from their nominal tuned points are also evaluated.

A. Impact of Q

A critical factor whose impact on the model needs to be carefully quantified is the unloaded Q's of L_2, $L_{\text{rec},2}$, and $C_{2\text{p}}$. In the previous section, these were assumed to be constant at $Q_{\text{L,UL}} = 400$ and $Q_{\text{C,UL}} = 2000$. However, it is known that these values change as currents flow through the system, causing the temperatures of the components in the system to increase. The authors in [25] showed the pad Q's can decrease by as much as 30% if energized for an extended period of time.

To fully quantify the impact variations in component Qs will have on the model, $Q_{\text{L,UL}}$ was varied over a wide range of $\pm 50\%$ from nominal (between 200 and 600). This range is larger than the typical range of Q for IPT pads to fully capture the impact of higher loss in the modeling technique presented. $Q_{\text{C,UL}}$ is varied between 1500 and 2500, which is a typical range for an 85 kHz capacitor tuning board.

The relative position of the two pads will cause variations in L_2, typically within 5% of the nominal value. $L_{\text{rec},2}$ also varies based on the construction of the inductor and changes over time due to increasing temperatures and physical shifts in the air gap.

The tuning board capacitors have an NP0 temperature coefficient, so are relatively resilient to changes in temperature and frequency. However, they will inevitably vary due to aging. This section quantifies how these variations impact the proposed model and investigates worst-case scenarios where the passive components are assumed to vary up to $\pm 10\%$ from their nominal values.

Table I shows that the built practical $C_{2\text{p}}$ differs from the ideal value by approximately 0.8%, and $C_{2\,\text{s}}$ has a variation of $\leq 0.4\%$. The biggest deviation from the nominal ideal values was $L_{\text{rec},2}$, but this was by design, and this deviation does not have a significant impact on P_{out}.

As shown in Fig. 2, the secondary pad and partial series compensation, which make up X'_{L2} as described in (8) is assumed to have an $Q_{\text{L,UL}} = 400$. Each component Q is varied independently, while the Q's of the other components are held at their nominal values. Both ΔP_{out} per V_{oc}, and $\Delta\theta_{12}$ are analyzed relative to their nominal values shown in Fig. 3 at the operating points given in Table III. The results of each of the Q variations are presented in Fig. 5 and show that it is critical to analyze the system using sensible Q's, similar to what would usually be expected in a well-constructed system; otherwise, there will be additional errors in the power and phase predictions.

Variations due to changes in the Q of the secondary pad impedance (X'_{L2}), denoted as Q_{L2}, have little impact on either overall output power per volt or θ_{12}, with variations generally between $\pm 1\%$ for power, and $< 0.1\%$ for θ_{12}. The general trend here is that the system will have a higher output power as Q_{L2} increases. As long as Q_{L2} is kept relatively high (> 300), then the system will deliver the desired output power. However, there is a P_{out} drop of up to 1% as Q_{L2} is halved from 400 to 200. If Q_{L2} continues to decrease, the system becomes less efficient, and P_{out} continues to drop.

The Q of the secondary rectifier inductor $Q_{\text{Lrec},2}$ has almost no impact on the output power or θ_{12}. However, it should be noted that higher Q's here will result in a lower system loss overall, so the design goal should be to keep $Q_{\text{Lrec},2}$ as high as possible in the practical build stage.

The unloaded Q of the secondary parallel capacitor $C_{2\text{p}}$ also has minimal impact on the output power per volt and θ_{12}. As discussed, these capacitors tend to have very high Q factors. In practice, the built capacitor board and the ideal $C_{2\text{p}}$ shown in Table I has a +0.7% difference. Assuming that the primary side does not change, Fig. 6 shows that P_{out} per V_{oc} increases by approximately 0.1% at the nominal position

These results confirm that higher Q's are better in terms of stability of power output and lower losses in the secondary side of the IPT system. Even large variations in Q only have small impacts on ΔP_{out} and θ_{12}.

B. Variation in Impedances

Equation (8) shows the secondary pad impedance is a sum of the impedances of the coil and the partial series capacitor. Here, the coil inductance varies more than $C_{2\,\text{s}}$, which is a fixed value once constructed. As such, the sensitivity study focuses on what happens to the system when L_2 varies, and the degree of variation is shown in (17). Here, $\Delta\omega L_2$ ranges between 0.9 and 1.1 times the nominal value presented in Table I

$$\Delta X'_2 = \omega\Delta L_2 + \omega L_{2,\text{lead}} - \frac{1}{\omega C_{2\,\text{s}}}. \tag{17}$$

In this study, a 10% change in L_2 equates to a difference of $\pm 26\%$ from the nominal X'_2. For the system analyzed in this article, this variation results in an overall range of 2.616–4.464 Ω. In practice, $L_2 + L_{2,\text{lead}}$ has a very low variation ($\leq 0.7\%$), and the practical impedance of $C_{2\,\text{s}}$ ($1/(\omega C_{2\,\text{s}})$) is only 0.36% lower than the ideal value.

The result of the sensitivity study is presented in Fig. 7 for the three operating conditions (A,C, and D) given in Table III as $X_{\text{L2}'}$, X_{Lrec2}, and X_{C2p} vary around the nominal values.

In the studied case, P_{out} per V_{oc} changes depending on the mistuning of the secondary pad's effective impedance. The measured X'_2 is equal to 3.63Ω, which is 2% higher than the ideal value. According to Fig. 7, this degree of mistuning results

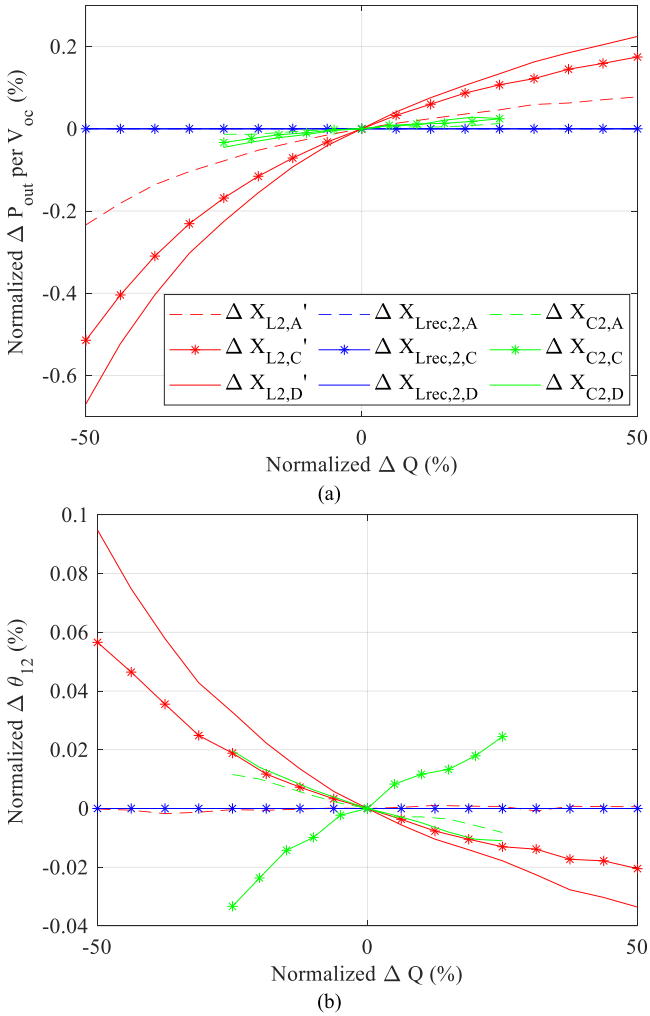

Fig. 6. Sensitivity study of (a) P_{out} per V_{oc} and (b) θ_{12} due to variations in inductor and capacitor Q's. The nominal operating points A, C, and D are shown in Table III and Fig. 3.

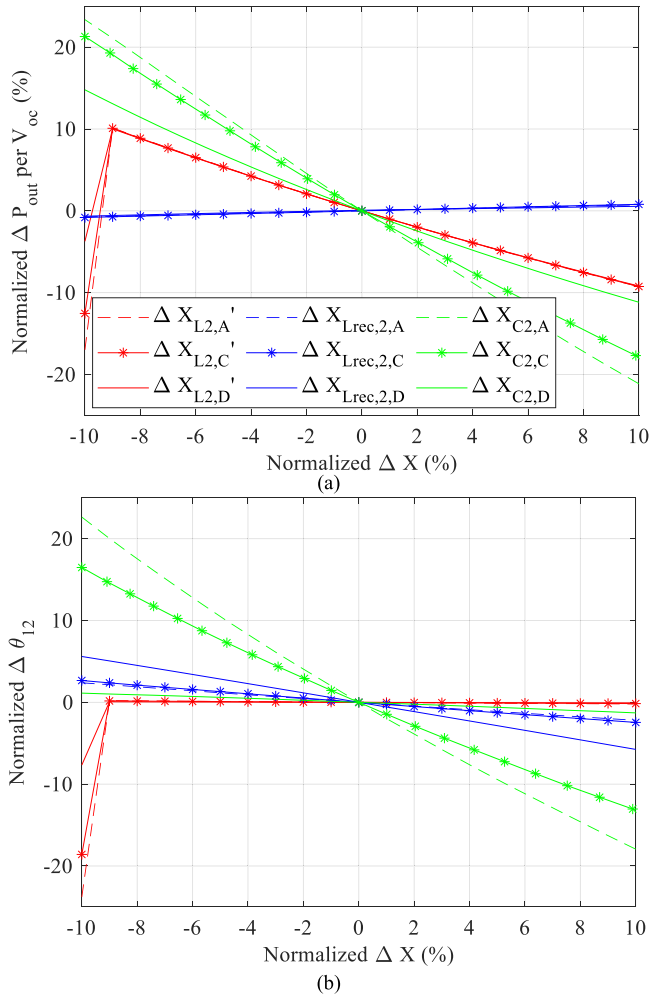

Fig. 7. Sensitivity study of (a) P_{out} per V_{oc} and (b) θ_{12} due to variations in inductor and capacitor impedances. The nominal operating points A, C, and D are shown in Table III and Fig. 3.

in an output power drop of approximately 1.1%, and the θ_{12} is expected to also drop approximately 0.9% for all three analyzed operating conditions.

Fig. 7 also shows that the P_{out} and θ_{12} drop caused by the mistuning X_2' is independent of the gain factors used to normalize the system. However, it is clear that there is a minimum detuning factor of approximately -9% where the output power begins to decrease to zero quickly. This suggests that if mistuning is unavoidable, it should be biased during construction by ensuring that X_2' and X_{C2p} are higher than the nominal values.

Furthermore, parasitic lead inductance plays a large role in the design of the system. Any design in higher power IPT systems need to be able to separate the inductance, which generates or captures flux and the parasitic lead inductance, which does not contribute to power transfer. If the lead inductance varies and is higher than expected, then there will be a power drop in the practical system. In any practical system, the magnetics need to be placed in predefined locations, and this is usually quite a large distance away from the electronic system. Any lead inductances need to be quantified properly, and the tuning network designed accordingly.

Mistuning of $C_{2\text{p}}$ has a different impact on P_{out} per V_{oc}. A lower capacitance translates to a higher impedance, and the errors that typically exist in a practical tuning board should be under $1\,\%$. For the system presented in this article, the actual mistuning is lower by $0.7\,\%$. A power increase of 2% is expected at point A, while approximately 1.3% is expected at points C and D relative to their nominal tuned results. Combined with the power drop due to the mistuning in X_2', an overall higher power delivery than originally expected is achieved. This agrees with the measured results presented in Table III, where all measured values follow a trend of being higher than the simulated values.

Similarly, θ_{12} also increases due to the higher $C_{2\text{p}}$. It is shown that mistuning has a larger impact on θ_{12} when $G_{\text{V}} \approx 3$ for the practical mistuning case compared to when G_{V} approaches 1, where the shift in θ_{12} approaches 0%. This aligns well with the measured phase shifts, which are all slightly higher than the simulated values.

TABLE IV
ERROR BETWEEN THE EXPERIMENTAL RESULTS AND SIMULATIONS USING PRACTICAL VALUES

	Point A		Point C	
	Sim	Error (%)	Sim	Error (%)
I_2 (A)	205.07	1	78.76	2.5
P_{out} (kW) (A)	48.7	1.5	9.27	-0.6
θ_{12} (°)	68.02	1.5	68.24	2.4
	Point D		Point E	
I_2 (A)	34.52	1.7	70.01	3.0
P_{out} (kW) (A)	4.23	-1.6	4.32	1.4
θ_{12} (°)	75.48	-2.6	67.65	2.0

Mistuning of the rectifier inductor does not have a significant impact on the P_{out} per V_{oc}. Even a large deviation here of up to +10% in this inductance only results in a P_{out} increase of under 1%. This is because if the secondary network made up of X_2', $X_{\text{Lrec,2}}$ and X_{C2} is relatively well tuned, then the rms value $I_{\text{rec,2}}$ should be very close to I_{sc}'. As such, ΔI_{out}, and therefore ΔP_{out} will be small.

Additional simulations have been performed using the real tuning values and are compared to the measured values shown in Table III. The simulated values and their errors from the measured values are given in Table IV. The results in this table show that the measured and the simulated results using practical values have consistently close agreement at all under 3%. However, it is difficult to predict the degree of mistuning at the design stage, and the proposed LUT method is proposed as a guide to help designers understand how the system performs with ideal values.

The power output continuously increases as X_{C2p} decreases. However, this result is due to the limited range shown. As X_{C2p} decreases further, the system becomes mistuned, and the power output decreases. This analysis shows that the two most important components to keep in tune include the effective secondary coil inductance and the parallel capacitor. For a practical design with good quality control, variations should be within 2% of the nominal design values, and therefore a worst-case 5% fluctuation in output power may be expected.

The absolute errors become increasingly impactful as the ratings of the IPT system increase. For the 50 kW system of interest, a 2% increase in X_2' results in a change in output power from 46.7 to 48 kW, as shown at point A. This suggests that as power levels increase, the accuracy of the tuning values themselves will be critical. For example, for a 250 kW system, a 0.7% increase in C_{2p} results in a P_{out} fluctuation of 2 kW.

VI. CONCLUSION

This article has shown that the proposed LUT method can be usefully used to characterize the secondary side of an IPT system that is *LCL*-tuned. It helps predict the output power, the phase shift between the primary and secondary currents, and the rms value of the secondary current itself. The proposed LUT is useful for understanding how phase shifts are impacted by the introduction of higher-order harmonics within the passive rectifier. The DCM boundary has also been found for the passive *LCL* secondary rectifier network.

This method allows designers to decouple the design of the secondary side of the IPT system from the primary side since the performance of the primary side can be abstracted into the value of V_{oc}. This means the secondary side parameters of interest can be determined independently, decreasing the simulation time and resulting in a faster overall design procedure.

A number of different operating conditions were investigated and validated. The work shows close agreement in both output power and phase shift of the primary and secondary currents over a wide power range.

A sensitivity analysis was performed and shows that a small amount of secondary mistuning will cause the *LCL*-tuned secondary power and θ_{12} to fluctuate. However, for a practical system, which is nominally well-tuned, the variations in power are stable ($\leq 5\%$).

REFERENCES

[1] H. Feng, R. Tavakoli, O. C. Onar, and Z. Pantic, "Advances in high-power wireless charging systems: Overview and design considerations," *IEEE Trans. Transport. Electrific.*, vol. 6, no. 3, pp. 886–919, Sep. 2020.

[2] G. A. Covic and J. T. Boys, "Inductive power transfer," *Proc. IEEE*, vol. 101, no. 6, pp. 1276–1289, Jun. 2013.

[3] "Power transfer for light-duty plug-in/electric vehicles and alignment methodology," SAE International, Warrendale, PA, USA, SAE J2954, 2020.

[4] M. Mohammad, O. C. Onar, V. Prakash Galigekere, G.-J. Su, and J. Wilkins, "Magnetic shield design for the double-D coil-based wireless charging system," *IEEE Trans. Power Electron.*, vol. 37, no. 12, pp. 15740–15752, Dec. 2022. [Online]. Available: https://doi.org/10.1109/TPEL.2022.3191911

[5] A. Kamineni, M. Neath, G. Covic, and J. Boys, "A mistuning-tolerant and controllable power supply for roadway wireless power systems," *IEEE Trans. Power Electron.*, vol. 32, no. 9, pp. 6689–6699, Sep. 2017.

[6] H. Hao, G. A. Covic, and J. T. Boys, "A parallel topology for inductive power transfer power supplies," *IEEE Trans. Power Electron.*, vol. 29, no. 3, pp. 1040–1151, Mar. 2014.

[7] C.-S. Wang, G. A. Covic, and O. H. Stielau, "Investigating an LCL load resonant inverter for inductive power transfer applications," *IEEE Trans. Power Electron.*, vol. 19, no. 4, pp. 995–1002, Jul. 2004.

[8] F. Lu, H. Zhang, H. Hofmann, W. Su, and C. C. Mi, "A dual-coupled LCC-Compensated IPT system with a compact magnetic coupler," *IEEE Trans. Power Electron.*, vol. 33, no. 7, pp. 6391–6402, Jul. 2018.

[9] F. Lu et al., "A low-voltage and high-current inductive power transfer system with low harmonics for automatic guided vehicles," *IEEE Trans. Veh. Technol.*, vol. 68, no. 4, pp. 3351–3360, Apr. 2019.

[10] J. M. Arteaga, S. Aldhaher, G. Kkelis, D. C. Yates, and P. D. Mitcheson, "Multi-MHz IPT systems for variable coupling," *IEEE Trans. Power Electron.*, vol. 33, no. 9, pp. 7744–7758, Sep. 2018.

[11] F. Lin, G. A. Covic, and M. Kesler, "Design of a SAE compliant multicoil ground assembly," *IEEE J. Emerg. Sel. Topics Ind. Electron.*, vol. 1, no. 1, pp. 14–25, Jul. 2020.

[12] P. A. J. Lawton, F. J. Lin, and G. A. Covic, "Magnetic design considerations for high-power wireless charging systems; magnetic design considerations for high-power wireless charging systems," *IEEE Trans. Power Electron.*, vol. 37, no. 8, pp. 9972–9982, Aug. 2022. [Online]. Available: https://dx.doi.org/10.21227/e2tf-5095

[13] H. Wang, U. Pratik, A. Jovicic, N. Hasan, and Z. Pantic, "Dynamic wireless charging of medium power and speed electric vehicles," *IEEE Trans. Veh. Technol.*, vol. 70, no. 12, pp. 12552–12566, Dec. 2021.

[14] C. Cai et al., "Design and optimization of load-independent magnetic resonant wireless charging system for electric vehicles," *IEEE Access*, vol. 6, pp. 17264–17274, 2018.

[15] Y.-G. Su, L. Chen, X.-Y. Wu, A. Patrick Hu, C.-S. Tang, and X. Dai, "Load and mutual inductance identification from the primary side of inductive power transfer system with parallel-tuned secondary power pickup," *IEEE Trans. Power Electron.*, vol. 33, no. 11, pp. 9952–9962, Nov. 2018.

[16] Y. Chen, S. He, B. Yang, S. Chen, Z. He, and R. Mai, "Reconfigurable rectifier-based detuned series-series compensated IPT system for anti-misalignment and efficiency improvement," *IEEE Trans. Power Electron.*, vol. 38, no. 2, pp. 2720–2729, Feb. 2023.
[17] W. Li, H. Zhao, S. Li, J. Deng, T. Kan, and C. C. Mi, "Integrated LCC compensation topology for wireless charger in electric and plug-in electric vehicles," *IEEE Trans. Ind. Electron.*, vol. 62, no. 7, pp. 4215–4225, Jul. 2015.
[18] H. Zeng, F. Peng, and U. Karki, "First order frequency-domain analytical model for resonant converters in CCM," in *Proc. IEEE Energy Convers. Congr. Expo.*, 2018, pp. 1997–2002.
[19] X. Zhang, T. Kan, C. You, and C. Mi, "Modeling and analysis of AC output power factor for wireless chargers in electric vehicles," *IEEE Trans. Power Electron.*, vol. 32, no. 2, pp. 1481–1492, Feb. 2017.
[20] C.-S. Wang, G. A. Covic, and O. H. Stielau, "Power transfer capability and bifurcation phenomena of loosely coupled inductive power transfer systems," *IEEE Trans. Ind. Electron.*, vol. 51, no. 1, pp. 148–157, Feb. 2004.
[21] T. Ma, C. Jiang, J. Xiang, X. Wang, K. T. Chau, and T. Long, "Modeling and analysis of wireless power transfer system via unified full-load discrete-time model," *IEEE Trans. Ind. Electron.*, vol. 70, no. 6, pp. 5626–5636, Jun. 2023.
[22] T. Diekhans and R. W. De Doncker, "A dual-side controlled inductive power transfer system optimized for large coupling factor variations," in *Proc. IEEE Energy Convers. Congr. Expo.*, 2014, pp. 652–659.
[23] M. Mohammad et al., "Bidirectional LCC-LCC compensated 20-kW wireless power transfer system for medium-duty vehicle charging," *IEEE Trans. Transport. Electrific.*, vol. 7, no. 3, pp. 1205–1218, Sep. 2021.
[24] H. H. Wu, A. Gilchrist, K. D. Sealy, and D. Bronson, "A high efficiency 5 kW inductive charger for EVs using dual side control," *IEEE Trans. Ind. Inform.*, vol. 8, no. 3, pp. 585–595, Aug. 2012.
[25] G. R. Kalra, M. G. S. Pearce, S. Kim, D. J. Thrimawithana, and G. A. Covic, "A power loss measurement technique for inductive power transfer magnetic couplers," *IEEE J. Emerg. Sel. Topics Ind. Electron.*, vol. 1, no. 2, pp. 113–122, Oct. 2020.

Feiyang J. Lin (Member, IEEE) received the B.E.(Hons.) degree in electrical and computer engineering and the Ph.D. degree in electrical engineering from The University of Auckland, Auckland, New Zealand, in 2012 and 2017, respectively.

He is currently a Senior Lecturer with the University of Auckland, working on the design of heavy duty wireless power systems for stationary and dynamic electric vehicle charging applications. He has been involved in the design of suitable magnetics to transfer power while meeting safety requirements, as well as developing power electronics hardware and software necessary to deliver regulated power safely. He has been involved in developing practical solutions for companies, such as WiTricity and Airbus.

Patrick A. J. Lawton (Student Member, IEEE) received the B.E. (first class Hons.) degree in electrical and electronic engineering in 2019 from the University of Auckland, Auckland, New Zealand, where he is currently working toward the Ph.D. degree in electrical and electronic engineering.

His research interests include wireless power transfer, high-power magnetics for inductive power transfer systems, and power electronics.

Grant A. Covic (Senior Member, IEEE) received the B.E. (Hons.) and Ph.D. degrees in electrical and electronic engineering from The University of Auckland (UoA), Auckland, New Zealand, in 1986 and 1993, respectively.

He was appointed as a full time Lecturer in 1992, a Senior Lecturer in 2000, an Associate Professor in 2007, and a Professor in 2013 with the Department of Electrical, Computer, and Software Engineering, UoA. In 2010, he cofounded (with Prof. John Boys) a new global start-up company "HaloIPT" focusing on electric vehicle (EV) wireless charging infrastructure, which was sold in late 2011. He currently heads inductive power research with the UoA and is directing a government funded research program on stationary and dynamic wireless charging of EVs within the road, while also coleading the interoperability subteam within the SAE J2954 wireless charging standard for EVs. He has authored or coauthored more than 200 refereed papers in international journals and conferences in the areas of his interest. He holds a number of patent families with many more pending, from which licenses in specialized application areas of inductive power transfer (IPT) have been granted around the world. His research and consulting interests include power electronics, EV battery charging, and resonant IPT.

Dr. Covic is a Fellow of both Engineering New Zealand and the Royal Society of New Zealand. He was the recipient of the Clean Equity Monaco Award for excellence in the field of environmental engineering, during this time at HaloIPT, and two NZ Clean Innovation Awards in the emerging innovator and design and engineering categories. He was also the recipient of the New Zealand Prime Minister's Science Prize, the Vice Chancellors commercialisation medal, and the KiwiNet Research Commercialization Awards for scientific research, which has seen outstanding commercial success. He was a Distinguished Lecturer for the IEEE Transportation Electrification Community, from 2016 to 2019, and is currently active on the steering committee for wireless power week.